Journal Name

ARTICLE

ZrO_2-SBA-15 catalysts for the one-pot cascade synthesis of GVL from furfural

Received 00th January 20xx,
Accepted 00th January 20xx

DOI: 10.1039/x0xx00000x

www.rsc.org/

J. Iglesias,*[a] J. A. Melero,[a] G. Morales,[a] M. Paniagua,[a] B. Hernández,[a] A. Osatiashtiani,[b] A. F. Lee[c] and Karen Wilson[c]

Controlling the thickness of zirconia monolayers coated over SBA-15 offers an effective way to tune catalytic performance for the acid-mediated and hydrogen transfer (Meerwein Ponndorf Verley, MPV) cascade transformation of furfural to γ-valerolactone. Complementary mechanistic and kinetic modelling establishes the existence of the two distinct zirconium active species (weak and strong acid sites), whose balancing enables optimisation of the cascade and hence maximal γ-valerolactone (GVL) production.

Introduction

Within the context of a bio-based economy, lignocellulosic biomass is an interesting and sustainable source of raw materials that provide solutions for the production of many different products conventionally obtained from crude oil, including transportation fuels and chemicals. This type of biomass can be transformed into sugar monosaccharides (glucose and xylose) that can be subsequently used to produce bio-fuels and bio-products. In general, such processes require several discrete chemical transformations, each usually driven by a specific class of catalyst to achieve the desired bio-product. Syntheses involving multiple intermediates and competing side reactions are difficult to commercialise at industrial scale, and hence there is growing interest in one-pot catalytic cascades to valorize sugars into platform chemicals.[1] This approach unlocks process advantages through the elimination of multiple separation and product work-up stages, but is also dependent on the discovery of new multifunctional catalysts able to promote each step along the reaction pathway.

Furfural is an abundant and low cost bio-derived product of xylose dehydration (the latter obtained from hemicellulose), and therefore an attractive building block to synthesise γ-valerolactone (GVL). GVL is an appealing compound due to its attractive physicochemical properties (low toxicity and biodegradability) and unique fuel characteristics. It can be directly used as food additive, green solvent, liquid fuel/additive for gasoline, and transformed into a wide collection of bioproducts, ranging from green fuels to bio-polymers.[2] GVL can be synthesized from furfural through a catalytic cascade of reactions (Scheme 1),[3] notably through the combination of acid and hydrogenation catalysts.[4-5] However, the use of molecular H_2 necessitates high operating pressures (typically >30 bar) and precious metal catalysts. Catalytic transfer hydrogenation by a Meerwein Ponndorf Verley (MPV) reaction, therefore represents a promising alternative route to reduce levulinic acid in GVL production.[6-8] Roman-Leshkov and co-workers reported GVL production from furfural by the combination of discrete Lewis and Brønsted catalysts (Zr-beta and Al-MFI zeolites) in the presence of isobutanol as a hydrogen donor.[9] Bifunctional Sn-Al and Zr-Al β-zeolite catalysts possessing both Lewis and Brønsted sites[10-14] were subsequently demonstrated to be active for the same reaction. Despite these promising results, and the simple post-synthesis protocol used to prepare such bifunctional zeolites,[15] their high manufacturing costs currently prohibits commercial exploitation for GVL production.

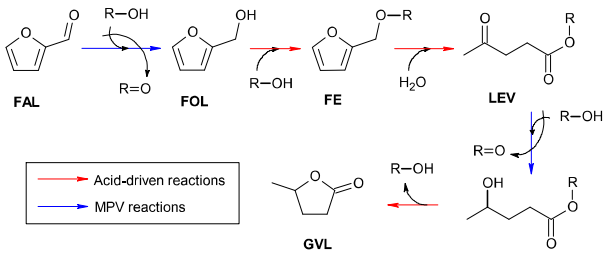

Scheme 1. Reaction scheme for the production of GVL from furfural by the combination of Lewis and Brønsted acid catalyst.

Zirconia is an abundant and low cost catalyst with relatively high acid and basic loadings,[16] properties that make it attractive for MPV reductions,[17,18] a key step in the GVL

[a] School of Experimental Sciences and Technology. Universidad Rey Juan Carlos, C/Tulipan. s/n. E-28933, Móstoles, Madrid, Spain.
[b] European Bioenergy Research Institute (EBRI), Aston University, Aston Triangle, Birmingham, B4 7ET, UK.
[c] School of Science, RMIT University, Melbourne, VIC 3001, Australia

† Electronic Supplementary Information (ESI) available: Catalyst characterisation and kinetic modelling results. See DOI: 10.1039/x0xx00000x

production from furfural. However, its naturally occurring dense form, zirconia exhibits poor textural properties which limit catalytic utility. Nevertheless, ZrO_2 coating of porous silicas (such as mesoporous SBA-15)[19] offers a simple way to enhance surface area and active site accessibility. In addition, ZrO_2-SBA-15 materials have been reported to be excellent catalysts for the MPV reduction of alkyl levulinates to GVL.[20,21] Here we take a further step, and demonstrate the application of ZrO_2-SBA-15 materials for the one-pot catalytic transformation of furfural into GVL. The combination of excellent textural properties, and ability to tune the solid acidity and H-transfer capability by altering the thickness of conformal ZrO_2 monlayers, enable optimisation of the overall cascade and GVL yields >30 %.

Experimental

Catalyst preparation

ZrO_2-SBA-15 was synthesized following our literature procedure:[19] 10 g pure SBA-15 silica was dried at 300 °C for 4 h before refluxing with 58.5g $Zr(OPr)_4$ (70 wt% in isopropanol, Aldrich) in 300 mL of anhydrous hexane. This method favors the reaction between surface hydroxyls (silanols) and zirconium propoxide resulting in a conformal ZrO_2 monolayer encapsulating the SBA-15 surface. Refluxing was performed overnight, and the resulting solid obtained by filtration then washed three times with hexane to remove any unreacted $Zr(OPr)_4$. Samples were subsequently rehydrated in 300 mL of deionised water under stirring for 4 h to fully hydrolyse residual propoxide groups, and provide new anchoring points for additional ZrO_2 monolayers. Samples were filtered and dried at 80 °C overnight, and the coating procedure repeated to obtain bilayer and trilayer zirconia coated SBA-15. Finally, samples were calcined at 550 °C in static air for 3 h, and denoted ZrO_2-SBA-15(1), ZrO_2-SBA-15(2), and ZrO_2-SBA-15(3) to reflect the number of ZrO_2 coatings. A Zr-SBA-15 reference, containing isolated zirconium sites within the mesostructured silica matrix, was also prepared through a direct synthesis procedure,[22] using a zirconocene dichloride (ABCR, 99 wt%) precursor.

Catalyst characterization

Textural properties were assessed by N_2 physisorption at 77 K using a Micromeritics TRISTAR 3000 porosimeter. Total pore volumes were recorded at P/P_0=0.985, and pore size distributions calculated by the BJH-KJS method. Mesoscopic ordering was evaluated by low-angle powder X-ray diffraction (XRD) on a PHILIPS X-PERT diffractometer using the Cu K_α line in the range 2θ = 0.6-5.0° with a step size of 0.02°. Phase identification was evaluated by wide-angle XRD in the range 2θ=10−90° with a step size of 0.04°. Bulk zirconium content was determined by ICP-OES. High-resolution transmission electron microscopy (HRTEM) was performed on a Philips TECNAI-20T microscope operated at 200 kV. X-ray photoelectron spectroscopy (XPS) was performed on a Kratos Axis HSi photoelectron spectrometer equipped with a charge neutralizer and Mg K_α X-ray source (hv = 1253.6 eV). Spectra were recorded at normal emission with an analyser pass energy of 20 eV and X-ray power of 225 W. ZrO_2 film thickness was calculated from attenuation of the Si 2p signal as previously described (see data in Table ESI-1). Acid loadings were determined by NH_3 temperature-programmed desorption (TPD) using a Autochem instrument (micromeritics). TPD profiles were fitted to calculate a maximum NH_3 desorption temperature and hence quantify acid strength. Base site loading was quantified by means of CO_2 pulse titration using a Quantachrome ChemBET instrument. Brønsted/Lewis acid character was calculated from diffuse reflectance FTIR spectroscopy (DRIFTS) of pyridine saturated samples under gas and liquid phase conditions. Infrared spectra were recorded on a Thermo Nicolet iS50 FT-IR spectrometer equipped with a LN_2 cooled MCT detector, and either Praying Mantis (gas phase) or ATR (liquid) attachments. DRIFT spectra were recorded on dry catalyst powders diluted in KBr onto which pyridine was dropped, and then dried in-vacuo overnight prior to analysis. The ATR liquid flow-through cell featured a trapezoidal, 10 bounce ZnSe crystal (80 mm×10 mmx4 mm). Spectra were the average of 120 scans recorded at room temperature and 4 cm^{-1} resolution, using the appropriate dried catalyst film for spectral background subtraction. Slurries of catalyst powders were prepared by adding 20 mg catalyst to 2 mL isopropanol and subsequent sonication for 15 min. 1 mL of slurry was then added dropwise to the ZnSe internal reflection element, and evaporated to obtain a uniform thin layer of catalyst over the ATR crystal. In-situ spectra of chemisorbed pyridine in the liquid phase were recorded by first passing a flow of isopropanol through the cell to saturate the catalyst surface for 1 h. A 0.1 vol% solution of pyridine in isopropanol was then introduced at 0.2 $ml.min^{-1}$ using a syringe pump for 1.5 h, and spectra of adsorbed pyridine then recorded.

Catalytic tests

The one-pot cascade transformation of furfural to GVL was performed in a 200 mL stainless steel, stirred autoclave fitted with a temperature controller and a pressure gauge. Reactions used 3.75 g furfural in a 1:50 molar ratio of furfural (Aldrich, 99 wt%) to isopropanol (Scharlab, 98 wt%), and 2.5:1 mass ratio of furfural to catalyst. Decane (Acros, 99 wt%) was added as an internal standard for reaction analysis at a concentration of 10 $g{\cdot}L^{-1}$. Catalysts were thermally treated in air at 450 °C for 5 h under static conditions prior to use. The reaction mixture was stirred at 1000 rpm, and heated to the desired temperature (130-170 °C) over a 1 h period. Aliquots of the reaction mixture were periodically withdrawn during 7 h for analysis.

Analysis of reaction products

The reaction mixture was analysed by gas chromatography using a Varian 3900 GC fitted with a CP-WAX column (30 mx0.25 mmx0.25 µm) and FID detector. Calibration curves were obtained from stock solutions, using decane as an internal standard, for furfuryl alcohol (FOL, Aldrich 98 wt%)

and γ-valerolactone (GVL, Aldrich 99 wt%). Isopropyl levulinate (i-LEV) was prepared according to methods described elsewhere,[23] and its purity assessed by ^{1}H and ^{13}C NMR. Catalyst performance was evaluated according to the following equations:

$$X_i = \frac{n_i^0 - n_i}{n_i^0} \cdot 100; \qquad Y_j = \frac{n_j}{n_i^0} \cdot 100$$

where X_i and Y_j are the mean conversion of i and yield towards j, respectively. Subscripts i and j denote reactants and products respectively, and superscript 0 refers to the initial conditions.

Results and discussion

Catalyst characterization and preliminary screening

Table 1 summarises the main physicochemical properties of the ZrO_2-SBA-15 materials, alongside commercial $ZrSiO_4$ (Zircon, Aldrich, 99 wt%), tetragonal ZrO_2 (Aldrich, 99 wt%), and the parent SBA-15. Layer-by-layer conformal growth of zirconia overlayers was previously evidenced by XPS, which revealed quantitative agreement between the predicted and experimentally determined Si 2p XP signal attenuation following the growth of the different ZrO_2 monolayers.[24] The observation of complete ZrO_2 monolayers suggests that adsorption of molecular Zr species is accompanied by the loss of multiple isopropoxide groups, possibly arising from partial hydrolysis by neighbouring silanols, which would increase the Zr concentration within each adlayer. Based on the unit cell dimensions of t-ZrO_2 two layers of ZrO_x octahedra are required to generate a structure with 'bulk-like' termination.

Table 1. Physicochemical properties of catalysts.

Catalyst	Zr loading (wt%)[a]	Textural properties		
		S_{BET} (m^2g^{-1})[b]	V_p (cm^3g^{-1})[c]	D_p (nm)[d]
t-ZrO_2	74.0	<5	0.01	-
$ZrSiO_4$	49.8	<5	0.01	-
Zr-SBA-15	8.4	533	1.26	12.3
SBA-15	-	451	1.18	11.1
ZrO_2-SBA-15(1)	17.0	367	0.75	8.3
ZrO_2-SBA-15(2)	24.4	349	0.57	6.7
ZrO_2-SBA-15(3)	30.0	296	0.43	6.5

[a]ICP-OES; [b]N_2 porosimetry; [c]Total pore volume for p/p_0=0.98;[d] Mean pore size from BJH-KJS method.

Zircon and tetragonal zirconia (t-ZrO_2) were highly crystalline (**Fig. ESI-1**) reflecting their correspondingly low surface area and porosity, and negligible acid loading (NH_3 TPD). In contrast, Zr-SBA-15 materials displayed a high surface area and large mesopore size, a moderate acid loading, and XRD reflections characteristic of only zircon domains.[22] Brønsted acidity in Zr-SBA-15 has previously been attributed to surface silanols, whereas Zr provides Lewis acidity[25-27]

ZrO_2-SBA-15 exhibited a sharp (100) reflection indicative of ordered mesopores within the parent SBA-15 for all ZrO_2 coated samples (**Fig. ESI-1A**), although the loss of (110) and (200) reflections suggests that surface modification by zirconia degrades the local ordering of mesopores in hexagonal arrays. Surface area and porosity progressively decreased with zirconia film thickness, resulting in a reduction in mesopore diameter and corresponding rise in wall thickness (**Fig. ESI-2**). TEM imaging confirmed that zirconia coated materials retained the hexagonal ordering of parallel mesopore channels present in the parent SBA-15 (**Fig. ESI-3**) which SEM imaging shows extend over hundreds of microns (**Fig. ESI-4**). No evidence of bulk ZrO_2 domains was observed for any ZrO_2-SBA-15 materials, although wide angle XRD reveals the emergence of small crystallites of t-ZrO_2 (**Fig. 1**) whose intensity slowly increase with film thickness.

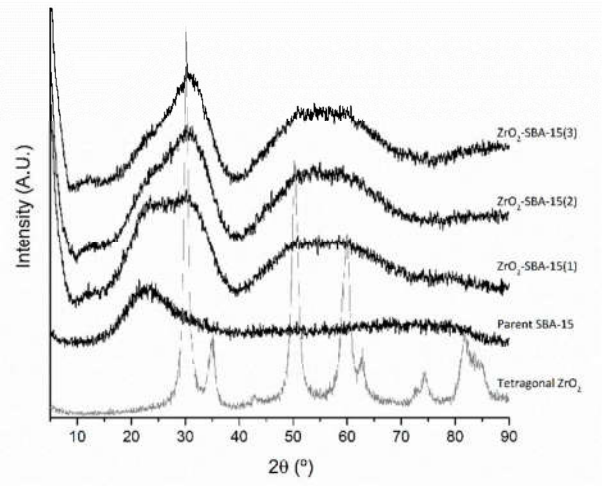

Fig. 1 Wide angle XRD patterns of ZrO_2-SBA-15, and pure SBA-15 and tetragonal ZrO_2

The zirconium chemical environment within ZrO_2-SBA-15 materials was subsequently explored by XPS (**Fig. 2**). Zr 3d XP spectra exhibit two distinct spin-orbit split components associated with the presence of interfacial Zr-O-Si and Zr-O-Zr species with $3d_{3/2}$ binding energies of 183.8 eV and 183.1 eV respectively, as previously reported.[19] The low binding Zr-O-Zr feature grows with film thickness, consistent with the formation of an ordered t-ZrO_2 phase observed by XRD, and the appearance of a low binding energy state in the O 1s spectra at 530.5 eV. Note that it is not possible to identify the presence of Zr-OH species, which would appear ~532 eV,[28] due to overlap by the intense, broad signal from the underlying silica substrate at 532.6 eV

Catalyst	Furfural conversion (mol %)	Product yield (mol %)[b]				
		FOL	i-FE	i-LEV	GVL	Total
t-ZrO_2	12	3	-	-	-	3
$ZrSiO_4$	9	<1	-	-	-	<1
Zr-SBA-15	86	1	40	14	1	56
ZrO_2-SBA-15(1)	99	11	62	7	2	82
ZrO_2-SBA-15(2)	93	5	60	6	3	73
ZrO_2-SBA-15(3)	90	13	60	4	3	79

[a]Reaction conditions: 130 °C, 7 h; furfural : 2-propanol=1:50 (by mols); furfural : catalyst=2.5:1 (by mass, equivalent to 10 g·L^{-1} catalyst). [b] Furfuryl alcohol (FOL); 2-propyl furfuryl ether (i-FE); 2-propyl levulinate (i-LEV); γ-valerolactone (GVL).

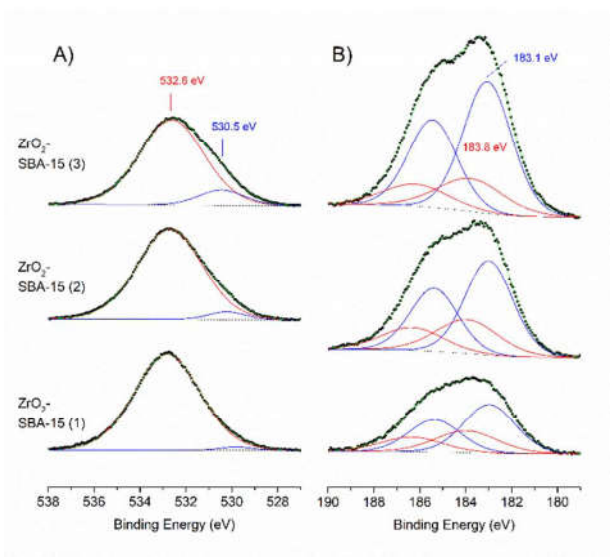

Fig. 2. (A) O 1s, and (B) Zr 3d XP spectra of ZrO_2-coated SBA-15.

Surface acidity of ZrO_2-SBA-15 materials was determined by NH_3 TPD (**Fig. ESI-5**) and pyridine adsorption (**Figure ESI-6-7**). Total acid loadings from ammonia titration increased from 0.227 to 0.357 $mmol_{eq}H^+ \cdot g^{-1}$ with ZrO_2 film thickness, accompanied by a concomitant decrease in acid strength (ammonia desorption temperature) summarised in **Table ESI-1**. The stronger (Lewis) acidity of zirconium cations at the interface with silica than within t-ZrO_2 is attributed to the greater electronegativity of silicon versus zirconium, and consequent stronger polarisation of interfacial Zr^{4+} cations.[29] The Brønsted/Lewis character of ZrO_2-SBA-15 materials was probed by both ex-situ (DRIFTS, **Fig. ESI-6**) and in-situ (ATR-IR, **Fig. ESI-7**) pyridine adsorption. Both measurements were in good quantitative agreement, with the Brønsted:Lewis ratio decreasing from ~0.3-0.4 to zero with increasing ZrO_2 film thickness (**Table ESI-1** and **2**). This observation is readily understood since Brønsted acidity is solely attributed to surface silanols,[25–27] which are capped by consecutive zirconia monolayers, the latter imparting Lewis acidity arising from undercoordinated Zr^{4+} sites. It is important to note that significant Lewis acid sites remain at the ZrO_2-SBA-15 surface even during immersion in isopropanol (**Fig. ESI-7**), the same solvent employed for our subsequent cascade reactions, and hence are catalytically relevant. This is an important finding, since the interconversion of Lewis to Brønsted acid sites has been previously proposed following alcohol adsorption over different metal oxides.[30]

Surface basicity assessed by CO_2 pulse chemisorption (**Table ESI-4**) revealed base site loadings orders of magnitude (0.002-0.011 mmol/g, **Table ESI-4**) lower than the corresponding acid site loadings (>0.205 mm/g), and hence is unlikely to contribute to the observed catalysis. It is also important to note that levulinic acid would rapidly neutralise such a low concentration of base sites during reaction. The extremely low basicity of our materials may reflect the use of a dry non-polar solvent in their synthesis (chosen to favour growth of ZrO_2 monolayers) compared with that of Kuwahara et al[20-21] who employed a polar solvent (which would likely favour ZrO_2 cluster formation).

Preliminary reactions were undertaken to benchmark the performance of ZrO_2-SBA-15 for the cascade transformation of furfural in isopropanol at 130 °C. The resulting furfural conversion and product yields are presented in **Table 2**.

Table 2. Furfural reaction over Zr catalysts.

Minimal furfural reduction occurred over commercial t-ZrO_2 and $ZrSiO_4$, presumably a consequence of their low surface area, in turn reflecting the stability of zirconium within the octahedral coordination geometry in these crystal structures; saturating the Zr coordination sphere limits opportunities for furfural and isopropanol binding, critical to the MPV mechanism.[31-33]

In contrast, Zr-SBA-15 and all ZrO_2-SBA-15 catalyst exhibit furfural conversions ≥86 %, attributable to the presence of undercoordinated Zr species either in the framework, at the interface with silica,[34] or within highly dispersed t-ZrO_2 crystallites.[32] Zr-SBA-15 material displayed a much lower catalytic performance in MPV reactions than ZrO_2-functionalized samples, as consequence of the lower concentration of Lewis acid sites in this material. Despite efficient furfural activation, neither Zr-SBA-15 nor any ZrO_2-SBA-15 produce high GVL yields, with furfuryl isopropyl ether (i-FE) the dominant product, formed by the condensation of furfuryl alcohol and the sacrificial isopropanol. The latter transformation requires acid sites, and is the dominant reaction over Zr-SBA-15 at 130 °C.[34] Isomerisation of furfuryl

isopropyl ether to i-propyl levulinate (i-LEV) is disfavoured under these conditions, consistent with reports that this transformation requires Brønsted acid sites.[9] The existence of an alternative (albeit slow) Lewis acid catalysed ring opening is, however, suggested by the increase in i-LEV yield with Lewis acid strength across the Zr- and ZrO_2-SBA-15 series. In any event, i-FE isomerisation to i-LEV appears rate-limiting. The final step in the reaction pathway from furfural to GVL is the reduction of the ketone group in i-LEV to yield 4-hydroxy-isopropyl valerate, and the latter's subsequent intramolecular transesterification (lactonisation) to GVL. Negligible 4-hydroxy-isopropyl valerate was detected, suggesting that reduction of the levulinate intermediate through H-transfer is the limiting stage, and thus, the GVL yield is controlled by the rate of the hydrogen transfer reaction. Despite the low GVL yields, ZrO_2-functionalized SBA-15 appears more active than Zr-SBA-15 for the MPV reaction, being favoured with each layer of ZrO_2 which provide increasing density of (weak) Lewis acid sites.

Temperature dependence and kinetic modelling

The influence of reaction temperature on the cascade transformation of furfural to GVL was further investigated over ZrO_2-SBA-15 catalysts between 130 to 170 °C in order to both optimise the process and provide extended datasets for kinetic modelling (**Fig. 3**). Complete furfural conversion was achieved in all cases in under 4 h, with the rate proportional to temperature. As anticipated, furfuryl alcohol (FOL) was the primary reaction product, and reached a maximum yield between 1 and 3 h, before decreasing at the expense of subsequent products in the cascade. The maximum FOL yield, and time at which this was attained, decreased with reaction temperature, suggesting that its rate of removal through etherification exhibits a strong temperature sensitivity. Furfuryl isopropyl ether (i-FE) is the next product observed, whose rates of formation and removal are again proportional to

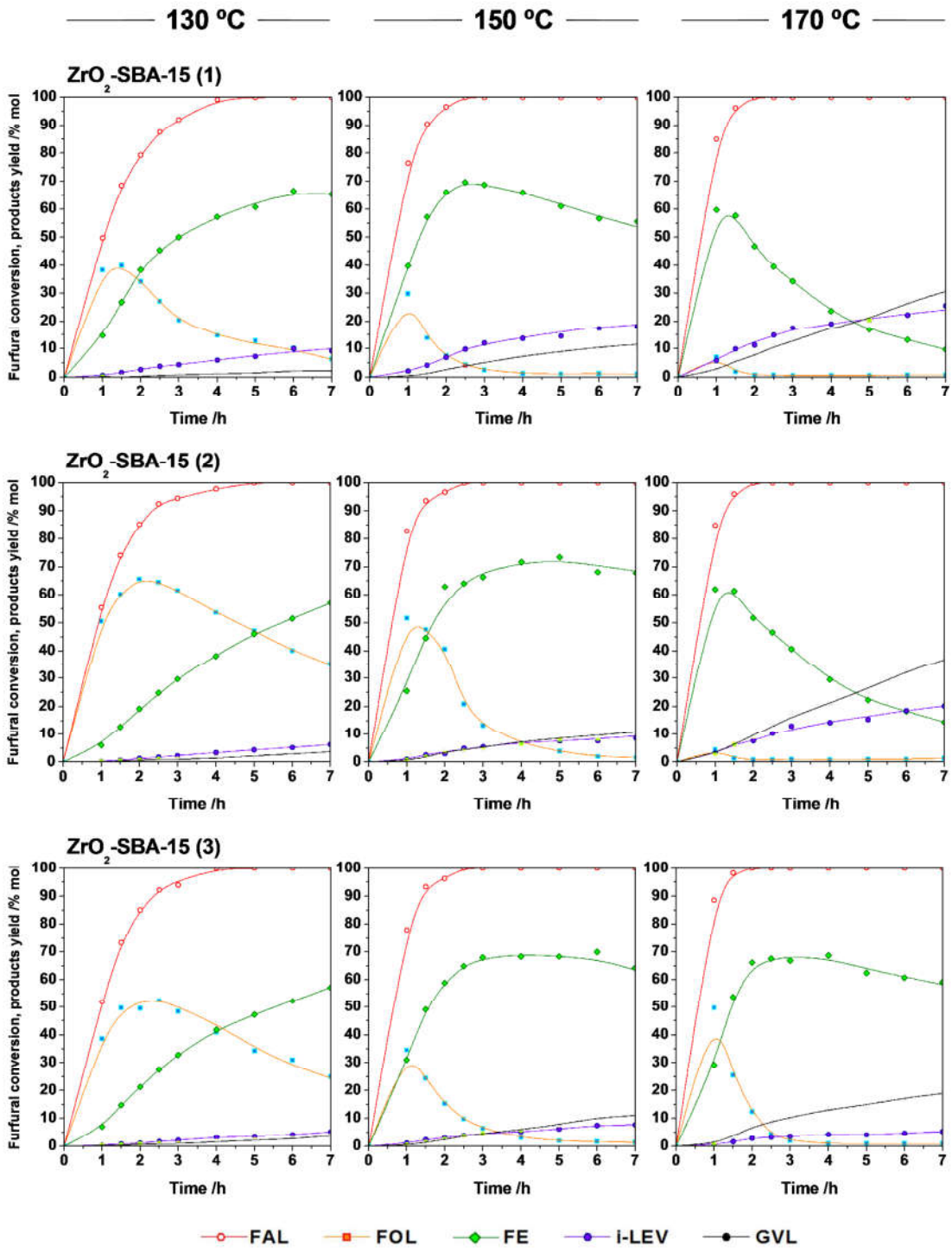

Fig. 3. Influence of temperature on the reaction of furfural over ZrO_2-SBA-15 catalysts. Reaction conditions: furfural:2-propanol=1:50 (by mols); furfural:catalyst=2.5:1 (by mass).

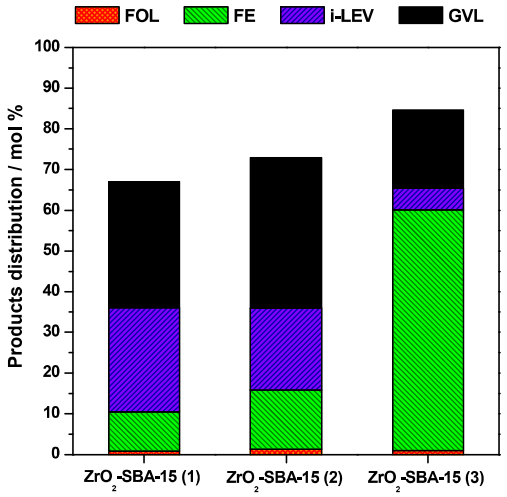

Fig. 4. Product distributions for the reaction of furfural over ZrO_2-SBA-15 catalysts. Reaction conditions: 170 °C; 7 h; furfural:2-propanol=1:50 (by mols); furfural:catalyst=2.5:1 (by mass).

temperature, although the latter remained relatively slow even at 170 °C, consistent with our hypothesis that isomerisation of the ether into isopropyl levulinate (i-LEV) is rate-limiting for the overall cascade. Since the maximum i-FE yield reached ~70 %, overcoming this bottleneck in the cascade could unlock efficient GVL production. i-LEV (slowly) accumulated at all temperatures, confirming that MPV reduction to form GVL was inefficient. Considering the impact of ZrO_2 film thickness, the mono- and bilayer functionalised SBA-15 catalysts showed increasing catalytic performance, being ZrO_2-SBA-15(2) slightly more efficient for the final MPV step at 170 °C, achieving the largest GVL yield for any system of 37 %. In contrast, the trilayer ZrO_2-SBA-15(3) catalyst proved ineffective for the isomerisation of i-FE to i-LEV even at 170 °C, consistent with its lack of Brønsted acid sites. The product distributions of the three ZrO_2-SBA-15 catalysts at 170 °C are summarised in **Fig 4**, which highlight that ZrO_2-SBA-15(2) offers good activity for furfural conversion to furfuryl alcohol, good rates of i-FE isomerisation, and modest rates of i-LEV reduction to GVL; we attribute this to its optimal balance of acid loading, strength, and trace Brønsted acidity. Undesired side reactions and resultant humin formation accounted for less than 15 % of the reactively-formed products over the more weakly acidic ZrO_2-SBA-15(2) and ZrO_2-SBA-15(3) catalysts, whereas stronger acid sites in ZrO_2-SBA-15(1) led to a poorer mass balance deficit of 33 % due to humin production.

A plausible reaction pathway for the cascade transformation of furfural into GVL in alcohol media over ZrO_2-grafted SBA-15 is proposed in **Scheme ESI-1**. Rate constants for each step can be derived by pseudo-homogeneous kinetic modelling, with the exception of 4-hydroxy isopropyl valerate lactonisation into GVL which is lumped together with the rate of i-LEV reduction, due to the rapid nature of the former intramolecular transesterification. Each step is fitted to a first-order equation, assuming stirred batch reactor operation, according to the following model equations for the reaction network:

$$\frac{dC_{FAL}}{dt} = -k_1 \cdot C_{FAL} - k_7 \cdot C_{FAL}$$

$$\frac{dC_{FOL}}{dt} = k_1 \cdot C_{FAL} - k_2 \cdot C_{FOL} - k_5 \cdot C_{FOL}$$

$$\frac{dC_{FE}}{dt} = k_2 \cdot C_{FOL} - k_3 \cdot C_{FE} - k_6 \cdot C_{FE}$$

$$\frac{dC_{i-LEV}}{dt} = k_3 \cdot C_{FE} - k_4 \cdot C_{i-LEV}$$

$$\frac{dC_{GVL}}{dt} = k_4 \cdot C_{i-LEV}$$

$$\frac{dC_H}{dt} = k_5 \cdot C_{FOL} + k_6 \cdot C_{FE} + k_7 \cdot C_{FAL}$$

where C is the molar concentration of each component, and k_i is the apparent rate constant of step i. and H designates humins. The Nelder-Mead method was used to optimise the rate constants through minimising the following objective function:

$$F_{obj} = \sum_m \left\{ \sum_{n=1}^{n_p} \left[C_{m,n,calc} - C_{m,n,exp} \right]^2 \right\}$$

were $C_{m,n,calc}$ and $C_{m,n,exp}$ are the calculated and experimental concentrations of component m at a given reaction time n. The resulting apparent first-order rate constants for the three ZrO_2-SBA-15 catalysts are reported in **Table ESI-5**. The proposed pseudo-first order kinetic model provides a good fit to the experimental datasets for all the catalysts (**Fig. ESI-8**).

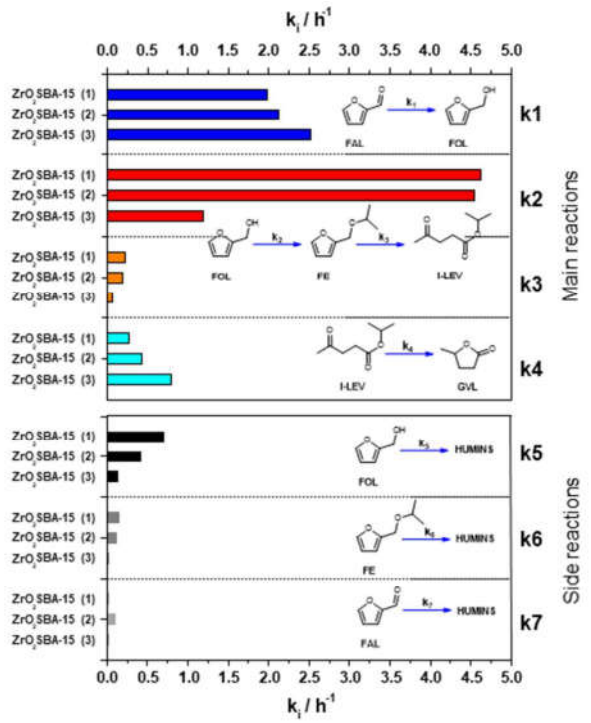

Fig. 5. Apparent first-order pseudo-homogeneous kinetic constants (ki) at 170 °C for steps 1, 2, 3, and 4 in the reaction of furfural over ZrO2-SBA-15 catalysts.

Furfural MPV reduction to furfuryl alcohol (k1) and its etherification with 2-propanol (k2) are the fastest steps over all catalysts, with furfuryl isopropyl ether isomerisation to isopropyl levulinate (k3) confirmed as rate-limiting in all cases. These findings are in accordance with the observed acid properties of our three ZrO_2-SBA-15 catalysts; the first and the last steps (MPV transformations) in the cascade sequence are Lewis acid, and base,[18,21] catalysed, while the intermediate etherification and isomerisation steps are favoured by Brønsted and strong Lewis acids.[9]

The impact of zirconia film thickness on GVL production can now be rationalised. ZrO_2-SBA-15(1) possesses the highest rate for furfuryl alcohol etherification (k2) and i-LEV isomerisation (k3), but it does not effectively promote MPV reductions of furfural (k1) and isopropyl levulinate (k4). In contrast, ZrO_2-SBA-15(3) is the best catalyst for MPV reduction, but is extremely inefficient for the intermediate steps in the cascade (etherification and isomerisation). Humin production (**Scheme ESI-1**, reactions 5-7) is favoured at higher reaction temperature, but remains a slow process over all catalysts. Under these conditions, the bilayer ZrO_2-SBA-15(2) catalyst occupies the 'Goldilocks zone', offering an activity that falls between the thinner and thicker zirconia coatings for every step in the cascade. Nevertheless, the rate of humin formation seems to correlate with the acid strength, being all the humin yielding transformations faster in presence of ZrO2-SBA-15(1). Tailoring the physicochemical properties of zirconia monolayers, notably their acid loading, acid strength, and Brønsted:Lewis character provides a simple approach to optimise reaction steps in the cascade transformation of furfural to GVL. Future work will address the challenge of preparing high area, high acid loading, ZrO_2-SBA-15 analogues that possess enhanced Brønsted acidity to further accelerate the (rate-limiting) isomerisation of furfuryl isopropyl ether to isopropyl levulinate.

Catalysts reusability

Catalyst reuse was assessed over four consecutive reactions for the ZrO_2-SBA-15(2) sample which showed highest activity for GVL production. The first three reaction cycles (170 °C, 7 h) were performed by a direct reuse of the catalyst, which was recovered by filtration after each cycle and simply air dried overnight without any re-activation treatment. The originally white sample progressively darkened to a brown colour on re-use, indicating the adsorption of reactively-formed organics (desired products and humins), as confirmed by TGA of the used catalyst after three reaction cycles (**Fig. ESI-9**). This colour change was accompanied by partial deactivation and an inability to convert furfuryl isopropyl ether into isopropyl levulinate (the most challenging reaction in the overall cascade); this step is catalysed by strong acid sites which are themselves most susceptible to poisoning. A subsequent thermal reactivation (550 °C calcination in air for 5 h) restored the original white colour of the catalyst, and recovered the original catalyst activity in a subsequent fourth reaction cycle (**Fig. 6**). Catalyst deactivation appears associated with adsorption of organic residues at strong acid sites.

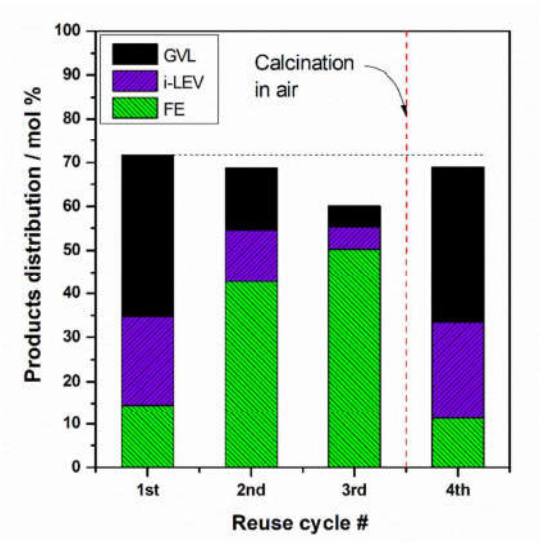

Fig. 6. Product distributions obtained with ZrO_2-SBA-15(2) in 4 consecutive reutilization cycles in the cascade transformation of furfural to GVL. Catalyst regeneration was accomplished by calcination in air after the 3rd reutilization cycle. Reaction conditions: 170 °C; 7 h; furfural:2-propanol=1:50 (by mols); furfural:catalyst=2.5:1 (by mass).

Conclusions

Conformal zirconia monolayers grown by a wet chemical route over mesoporous SBA-15 silica offer a flexible catalytic solution to drive the one-pot cascade transformation of furfural into GVL in isopropanol. The zirconia coatings contain two Zr species, those at the interface with silica and those within highly dispersed t-ZrO_2 crystallites prevalent in bi- and trilayers, associated with strong and weak acid sites respectively. Pyridine titration in vacuo and during immersion in isopropanol evidences predominantly Lewis acidity for all zirconia monolayer thicknesses; a small concentration of Brønsted acid sites observed for a single zirconia monolayer are probably associated with residual surface silanols. Furfural reduction and etherification with isopropanol is quite efficient at 130 °C, however a reaction temperature of 170 °C is required to drive the subsequent reaction steps.

Kinetic modelling of furfural reactivity over ZrO_2-SBA-15 catalysts identifies two distinct regimes associated with the strong and weak acid Zr species. Interfacial, strong Lewis acid Zr species within the first monolayer favour etherification and isomerisation of reactively-formed furfuryl alcohol but show poor activity for hydrogen transfer (MPV) chemistry. In contrast, more abundant, but weaker Lewis acid sites in t-ZrO_2 present in the bi- and trilayers promote furfural reduction and the MPV reduction of isopropyl levulinate to GVL. A zirconia bilayer coating, ZrO_2-SBA-15(2), offers the optimum balance of acidity and MPV hydrogen transfer activity to drive the cascade transformation of furfural to GVL with 37 % overall yield. Isomerisation of isopropyl furfuryl ether (formed by etherification of furfuryl alcohol) to isopropyl levulinate is the rate-limiting step in GVL production, suggesting that increasing the GVL yield will require either a higher density of strong Lewis sites or the stabilisation/introduction of additional Brønsted acidity. our catalytic tests were (deliberately) performed under dilute conditions with a view to minimize side reactions. Humin by product formation remains a challenge, and further work is required to optimise ZrO_2-SBA-15 catalysts for the selective transformation from furfural to GVL. Although other catalytic systems (e.g. Zr-Al-β zeolite)[12] display superior GVL selectivity, these much more expensive and difficult materials to synthesise. Finally, it is important to note that our experiments were conducted in the presence of excess solvent, and that such operation would decrease the profitability of any corresponding industrial process, since a large fraction of the feedstream would be constituted by the isopropanol solvent (although much of this could be recovered and recycled). Ongoing research is directed at reducing the amount of solvent through process optimisation.

Acknowledgements

Financial support from the Spanish Ministry of Economy and Competitiveness through the project CTQ2014-52907-R, as well as from the Regional Government of Madrid through the project S2013-MAE-2882 is gratefully acknowledged. B. Hernández thanks the Spanish Ministry of Economy and Competitiveness for a FPI grant (BES-2012-061144). Authors gratefully acknowledge M.Eng. P. Juárez for assistance in catalysts recycling study.

References

1 I. Delidovich, K. Leonhard, R. Palkovits, *Energy Environ. Sci.*, 2014, **7**, 2803.
2 K. Yan, Y. Yang, J. Chai, Y. Lu, *Appl. Catal. B Environ.*, 2015, **179**, 292–304.
3 R. Xing, W. Qi, G.W. Huber, *Energy Environ. Sci.*, 2011, **4**, 2193.
4 D. Ding, J. Wang, J. Xi, X. Liu, G. Lu, Y. Wang, *Green Chem.*, 2014, **16**, 3846.
5 J. Cui, J. Tan, T. Deng, X. Cui, H. Zheng, Y. Zhu, Y. Li, *Green Chem.*, 2015, **17**, 3084–3089.
6 M.J. Gilkey, B.J. Xu, *ACS catalysis*, 2016, **6**, 1420-1436.
7 M. Chia, J.A. Dumesic, *Chem. Commun.*, 2011, **47**, 12233.
8 R.S. Assary, L.A. Curtiss, J.A. Dumesic, *ACS Catal.*, 2013, **3**, 2694–2704.
9 L. Bui, H. Luo, W.R. Gunther, Y. Roman-Leshkov, *Angew. Chemie - Int. Ed.*, 2013, **52**, 8022–8025.
10 M.M. Antunes, S. Lima, P. Neves, A.L. Magalhães, E. Fazio, A. Fernandes, F. Neri, C.M. Silva, S.M. Rocha, M.F. Ribeiro, M. Pillinger, A. Urakawa, A. A. Valente, *J. Catal.*, 2015, **329**, 522–537.
11 M.M. Antunes, S. Lima, P. Neves, A.L. Magalhães, E. Fazio, F. Neri, M.T. Pereira, A.F. Silva, C.M. Silva, S.M. Rocha, M. Pillinger, A. Urakawa, A.A. Valente, *Appl. Catal. B Environ.*, 2016, **182**, 485–503.
12 J.A. Melero, G. Morales, J. Iglesias, M. Paniagua, C. López-Aguado, K. Wilson, A. Osatiashtiani, *Green Chem.*, 2017, **19**, 5114-5121.
13 H.P. Winoto, B.S. Ahn, J. Jae, *J. Ind. Eng. Chem.*, 2016, **40**, 62–71.
14 S. Song, L. Di, G. Wu, W. Dai, N. Guan, L. Li, *Appl. Catal. B Environ.*, 2017, **205**, 393–403.
15 C. Hammond, S. Conrad, I. Hermans, *Angew. Chemie Int. Ed.*, 2012, **51**, 11736–11739.
16 T. Viinikainen, H. Rönkkönen, H. Bradshaw, H. Stephenson, S. Airaksinen, M. Reinikainen, P. Simell, O. Kraus, *App. Catal. A: General*, 2009, **362**, 169-177.
17 C. Battilocchio, J.M. Hawkins, S.V. Ley, *Org. Lett.*, 2013, **15**, 2278-2281.
18 T. Komanoya, K. Nakajima, M. Kitano, M. Hara, *J. Phys. Chem. C*, 2015, **119**, 26540-26546.
19 G. Morales, A. Osatiashtiani, B. Hernández, J. Iglesias, J. A. Melero, M. Paniagua, R. Brown, M. Granollers, A.F. Lee, K. Wilson, *Chem. Commun.*, 2014, **50**, 11742–11745.
20 Y. Kuwahara, W. Kaburagi, T. Fujitani, *Bull. Chem. Soc. Jpn.*, 2014, **87**, 1252–1254.
21 Y. Kuwahara, W. Kaburagi, Y. Osada, T. Fujitani, H. Yamashita, *Catal. Today*, 2017, **281**, 418-428.
22 J.A. Melero, L.F. Bautista, J. Iglesias, G. Morales, R. Sánchez-Vázquez, *Cat. Today.*, 2012, **195**, 44-53.
23 H.J.M. Bosman, E.C. Kruissink, J. Vanderspoel, F. Vandenbrink, *J. Catal.*, 1994, **148**, 660-672.
24 A. Osatiashtiani, A.F. Lee, M. Granollers, D.R. Brown, L. Olivi, G. Morales, J.A. Melero, K. Wilson, *ACS Catalysis*, 2015, **5**, 4345-4352.
25 M. M. Antunes, P. Neves, A. Fernandes, S. Lima, A. F. Silva, M. F. Ribeiro, C. M. Silva, M. Pillinger and A. A. Valente, *Catal. Sci. Technol.*, 2016, **6**, 7812–7829.

26 J.A. Melero, L.F. Bautista, J. Iglesias, G. Morales, R. Sánchez-Vázquez, *Catal. Today*, 2012, **195**, 44–53.
27 J. Geboers, X. Wang, A.B. de Carvalho, R. Rinaldi, *J. Mol. Catal. A Chem.*, 2014, **388**, 106–115.
28 Y. Mi, J. Wang, Z. Yang, Z. Wang, H. Wang, S. Yang, *RSC Adv*. 2014, **4**, 6060-6067.
29 J.A. Anderson, C. Fergusson, I. Rodríguez-Ramos, A. Guerrero-Ruiz, *J. Catal.*, 2000, **192**, 344-354.
30 E. V. Beletskiy, X. Hou, Z. Shen, J. R. Gallagher, J. T. Miller, Y. Wu, T. Li, M. C. Kung,H. H. Kung, *J. Am. Chem. Soc.*, 2016, **138**, 4294–4297.
31 A. Corma, M. E. Domine, S. Valencia, *J. Catal.*, 2003, **215**, 294–304.
32 J. C. van der Waal, K. Tan, H. van Bekkum, *Catal. Letters*, 1996, **41**, 63–67.
33 F. Gonell, M. Boronat, A. Corma, *Catal. Sci. Technol.*, 2017, **7**, 2865, 2873.
34 J. Iglesias, J. A. Melero, G. Morales, J. Moreno, Y. Segura, M. Paniagua, A. Cambra, B. Hernández, *Catalysts*, 2015, **5**.